Next Materials 8 (2025) 100807

Contents lists available at ScienceDirect

Next Materials

journal homepage: www.sciencedirect.com/journal/next-materials

Research article

Multi-layer graphene powder (without metal nanoparticles) booster carbon supported platinum-tin electrocatalyst for the ethanol oxidation reactions

Tarso L. Bastos [a,1], Rogério V. Gelamo [b,2], Flavio Colmati [a,c,*,3]

[a] Universidade Federal de Goiás, Instituto de Química (IQ-UFG), Av. Esperança sn, Campus Samambaia, Goiânia, GO 74690-900, Brazil
[b] Universidade Federal do Triângulo Mineiro, Instituto de Ciências Tecnológicas e Exatas (ICTE-UFTM), Av. Doutor Randolfo Borges Junior, 1250, Uberaba, MG 38064-200, Brazil
[c] Centro de Excelência em Hidrogênio e Tecnologias Energéticas Sustentáveis (CEHTES), Rodovia R2 sn, Campus Samambaia - UFG, Goiânia, GO 74690-631, Brazil

ARTICLE INFO

Keywords:
Carbon allotrope
Catalyst activity
DEFC
Electrocatalysis
Graphene
Oxidation enhancement
Support

ABSTRACT

The Fuel Cell developments during recent years due to the world search renewable energy sources, has brought greats advantages to the devices. The world search for renewable energy sources brought great development to Fuel Cells during recent years. Nevertheless, the wide-scale use of these devices lacks the easiness production methods. This study investigated the blend of electrocatalyst and graphene powder aiming higher electrochemical activity in ethanol oxidation. The graphene powder obtained by thermal expansion was physically mixed with electrocatalyst PtSn/C synthesized by chemical reduction and the electrochemical activity of the electrocatalyst was tested in a three electrodes electrochemical cell. The results showed that the graphene amount without metal nanoparticles can directly influences in catalytic activity, increasing the current density of electrocatalyst. Furthermore, the durability and electrochemical characteristics are also enhanced, achieving best performance at 10-wt% graphene amounts. Promoting an enhancement of 34 % in the current density in acid (238.07 $mA{\cdot}mg_{Pt}^{-1}$), and 10 % in the alkaline electrolyte (225.24. $mA{\cdot}mg_{Pt}^{-1}$), in comparison to the standard electrocatalyst (without graphene). Therefore, this method has proven itself as simple and powerful toward enhancement of ethanol oxidation reactions.

1. Introduction

The emerging use of energy by humankind highlights the constant and increscent need for higher efficiency energy sources. Besides, the environment concern, sustainability and green energy raise fuel cells research in the recent years due high electrical energy generation producing water, and their portable applications as source of electric devices [1]. Direct alcohol fuel cells (DAFC) present a wide range of advantages among others fuel cell systems, as quick start-up, large fuel sources, high energy density and cost effective [2,3]. The use of alcohol as fuel brings additional advantages, as its oxidation reactions potentials are close to those of hydrogen, and it can achieve an open circuit potential higher than 1 V [4–6]. Nevertheless, utilizing ethanol requires highly efficient electrocatalysts capable of cleaving the C–C bond and facilitating the oxidation pathways that maximize electron transfer, closer to theoretical maximum, e.g. 12 electrons [7,8]. Through that, the electrocatalyst efficiency enhancement is essential to long term fuel cell applications as energy source devices.

Platinum is the most used catalyst to alcohol oxidation reaction (EOR), and hydrogen oxidation reaction (HOR) in fuel cells [9,10]. Unfortunately, for EOR it is easily susceptible to poisoning by-products of incomplete alcohol oxidations, such as CO [11,12]. The Pt electrocatalyst on EOR is directly correlated with the structure, size, morphology, surface oxidation state of the metal, even more, the metal alloy composition in the electrocatalyst [13,14]. The adding of a second, third or fourth metal to Pt-based aims avoid poisoning at same time that increases catalytic activity achieving better reactions kinetics [15,16]. Bi, Ni, Fe, Cu, Pd, Rh, Au, Zn and Mn are listed as most common elements presents in Pt-based alloy. The structure and molar metal ratio are directly related to better electrochemical surface area (ECSA), onset

* Corresponding author at: Universidade Federal de Goiás, Instituto de Química (IQ-UFG), Av. Esperança sn, Campus Samambaia, Goiânia, GO 74690-900, Brazil.
E-mail address: colmati@ufg.br (F. Colmati).
[1] 0000-0002-2357-3149
[2] 0000-0003-2124-3450
[3] 0000-0002-1867-0091

https://doi.org/10.1016/j.nxmate.2025.100807
Received 4 April 2025; Received in revised form 12 May 2025; Accepted 5 June 2025
Available online 13 June 2025

oxidation potential and current density peaks. Although, some structures such as nanowires, nanospheres, core-shell, hollow structures, skins monolayers and nanotubes will require different methods to be produced [17–22]. Such methods could be complex, laborious and high cost, which mitigates the affordable use of fuel cells as source energy to most devices. Another approach is to focus on support where the metal is anchored. The majority of electrocatalyst use carbon back the mainly support, though many researchers doping the surface with non-metals elements or functional groups aiming enhance the electrocatalyst performance [23–25]. The change of support material had been presented as a promising method to obtain higher performances by electrocatalyst. Using carbon allotropes, such as nanotubes, fibers and graphene [26, 27]. Nonetheless the performance enhancement by the use and blend of this materials, the laborious and often expensive methods to synthesized prolongs the research to better electrocatalysts [28–30]. Hence, this study proposes a new perspective to increases the electrocatalyst performance using a physical mixing of Pt_2Sn electrocatalyst supported on Vulcan carbon and different amount of the multilayer graphene sheet without metal contain.

2. Experimental

The Pt_2Sn electrocatalysts were prepared by chemical reduction of the metallic ions in solution, using $H_2PtCl_6.6H_2O$ Sigma-Aldrich® and $SnCl_2.2H_2O$ Sigma-Aldrich® as metals precursors, for a Pt-Sn molar ration of 2:1. The metal precursors and support (Carbon Vulcan XC-72R, Cabot 240 $m^2\ g^{-1}$) suspended in water/isopropyl solution and added dropwise 25 mL of $NaBH_4$ 0.05 M, stirring by 2 h and added dropwise more 25 mL of 0.1 M $NaBH_4$, with a total reaction time of 4 h. The electrocatalysts were filtered, washed with deionized water, and dried at 60 °C by 2 h, all electrocatalyst were prepared with 80 wt% of support (Carbon Vulcan) and 20 wt% of metals (Pt and Sn at 2:1 molar%) [31, 32].

The Pt_2Sn/C prepared earlier was separated into several samples and each one sample was added an amount of the multilayer Graphene (G) sheets for obtain $Pt_2Sn/C + G$. The G was prepared from natural graphite flakes thermally expanded. Nacional de Grafite Ltda Corporation donated the graphite samples. In order to exfoliate the graphite powder to obtain MLG dispersion, a mechanical process was conducted using ultrasound and organic solvents for 3 h. The MLG pellets were follows submitted to a new process, a further treated in isopropyl alcohol dispersion by ultrasound until producing multilayer graphene powder (G) [33,34].

The materials were characterized by XRD diffraction using a Shimadzu XRD-6000 diffractometer working with 40 kV and 30 mA and Cu K α radiation (wavelength, λ = 1540 Å). The crystallite average diameters (c) were determined by Scherrer equation, and the lattice parameters (*a*) were calculated by Bragg's law. Scanning electron microscopy (SEM) images were obtained on a Jeol JSM7100F field emission scanning electron microscope with an electron accelerating voltage of 5 kV in secondary electron detection mode. Compositional analyzes were carried out using the energy dispersive spectroscopy (EDS) technique, with an Oxford Instruments XMax-n 80 X-ray detector coupled to the microscope. The Transmission electron microscopy (TEM) was performed using a TEM microscope JEOL JEM 2100, URP operating at 200 kV and having a resolution of 0.2 nm. The samples for TEM were prepared by drop-casting an isopropyl alcohol suspension of the as-prepared catalysts over a carbon-coated copper grid (400 mesh and 3 mm diameter), followed by drying under ambient conditions. About 300 particles were measured to build the size distribution histograms. The mean particle diameter, (d), was calculated using Eq. 1.

$$d = \sum_k \frac{n_k d_k}{n_k} \quad (1)$$

Electrochemical characterizations were performing in a three electrodes electrochemical cell with a Pt gauze counter electrode, and $Ag/AgCl/KCl_{sat}$ as reference electrode for acid medium and the saturated calomel electrode (SCE) was used as reference for alkaline electrolyte. The measurements were carried out an Autolab potentiostat/galvanostat PGSTAT 302 N at room temperature (~ 27 °C) in 0.5 M H_2SO_4 (Sigma-Aldrich) and 1.0 M NaOH (Sigma-Aldrich) both with four ethanol concentration in the electrolyte. Aiming to analyze the influence of the MLG powder on the catalyst activity of ethanol oxidation, a physical mixing of the electrocatalyst and the multilayer graphene powder were prepared. The total mass was set up as 5 mg to prepare the suspension, varying the amount of both, as shown in Table 1.

The working electrode was prepared by an aliquot of 35 μL of a suspension dispersing into 1.4 mL of water, 1.0 mL of ethanol and 0.1 mL of Nafion® 117 solution (sigma Aldrich), deposited on glassy carbon (geometric area is 0.385 cm) imbibed in Teflon® rod and dried before electrochemical experiments. The electrochemical experiments performed were cyclic voltammetry (CV) in absence and presence of the different ethanol concentration in the electrolyte and chronoamperometry (CA) for available the electrochemical activity and stability.

3. Results and discussion

The chemical composition of the electrocatalyst was determined by using energy dispersive spectroscopy (EDS) technique. The spectra analysis in Fig. 1a shows the presence of platinum and tin in an atomic ratio close to 2:1, indicating the efficiency of the synthesis method. Fig. 1b presents the X-ray diffraction (XRD) patterns of Pt_2Sn/C, where 2θ peaks around 27°, 40°, 47° and 67° can be associated to Miller indices C(002), Pt(111), Pt(200) and Pt(220), respectively. The Miller indices C (002) can be assigned to the carbon amorphous structure, while Pt Miller indices indicate the face-centered cubic (fcc) crystallinity structure. Table 2 shows the lattice parameters and crystallite size calculated from the platinum peaks. The morphological structure can be confirmed by the standard Pt(220) lattice parameter, value assigned as 3.92 [35].

Fig. 2 presents the transmission electron microscopy (TEM), high-resolution transmission electron microscopy (HRTEM) and the histogram of the particle diameter frequency. Moreover, the particle size distribution follows a gaussian fitting [36] to measure the average particle diameter of the electrocatalysts, as shown in Table 2. Although some agglomeration (black dots) Fig. 2a shows a reasonable distribution of the metal alloy particles in the carbon support, while Fig. 2b shows the crystallinity of metal particles. A reasonable distribution and crystallinity of particles leads to a better chemical activity toward oxidation reactions. The histogram exhibits the particles diameter frequency measured from TEM imagens. The Gaussian distribution obtained an R^2 of 0.9943, measuring the average particle size as 4.54 nm, shown in Table 2.

Fig. 3a presents the XRD of multilayer graphene powder synthetize used in the physical mixing. The graphene structure was extensively studied and characterized in previous studies, proving the purity obtained by this method[34]. Then, the absence of other Miller indices peaks than C(002) and C(004) indicates the presence of only carbon elements and the crystalline morphology of graphene structure, different that amorphous presented by carbon Vulcan as electrocatalyst support (Fig. 1b). Along with theses, EDS (Fig. 3b) evidences the absence

Table 1
Graphene amount by electrocatalyst mass in the physical mixing.

Physical Mixing	Electrocatalyst (mg)	Graphene (mg)	Ratio (% m/m)
$\mathbf{Pt_2Sn/C_{100\,\%}}$	5.00	0.00	0 %
$\mathbf{Pt_2Sn/C_{90\,\%} + G_{10\,\%}}$	4.50	0.50	11 %
$\mathbf{Pt_2Sn/C_{80\,\%} + G_{20\,\%}}$	4.00	1.00	25 %
$\mathbf{Pt_2Sn/C_{60\,\%} + G_{40\,\%}}$	3.00	2.00	67 %
$\mathbf{Pt_2Sn/C_{40\,\%} + G_{60\,\%}}$	2.00	3.00	150 %
$\mathbf{Pt_2Sn/C_{20\,\%} + G_{80\,\%}}$	1.00	4.00	400 %

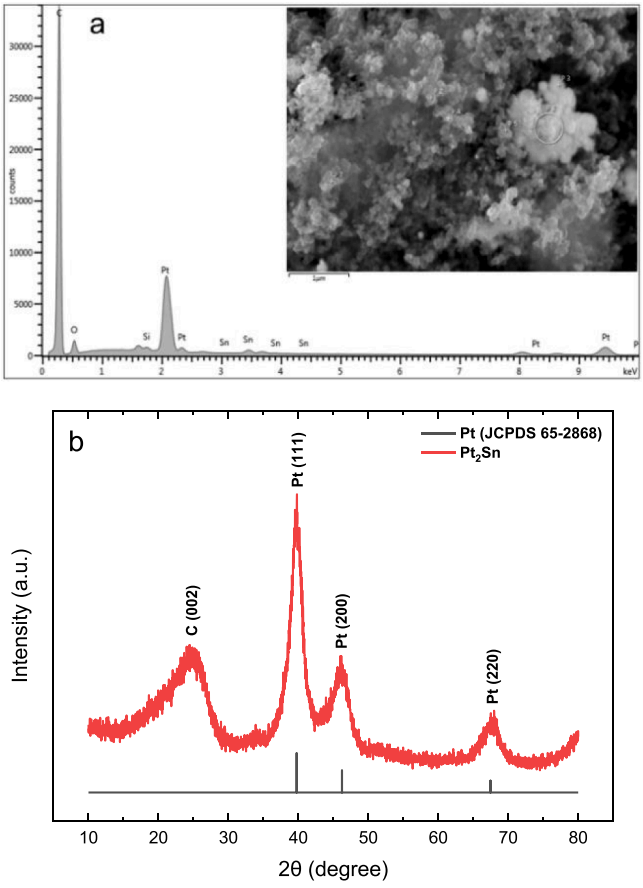

Fig. 1. (a) EDS spectra and (b) X-Ray diffractogram of Pt_2Sn/C. The standard patterns of pure Pt (JCPDS 65–2868) are attached for comparison. The inset shows a representative SEM image.

Table 2
Electrocatalyst lattice parameter, crystallite size, and particle size.

Miller indices	Lattice parameter / nm	Crystallite size / nm	Metallic particles size / nm
Pt(220)	0.392 ± 0.0198	3.36 ± 0.0554	4.54 ± 0.0024

of elements impurities on the graphene. The morphology of multilayers graphene sheets (Fig. 3c) exhibits a size over 50 μm, which is above 500 times greater than the carbon Vulcan particles size, usually varies between 20 and 100 nm, as showed in Fig. 2a. This could suggest graphene, usually in lower proportion mass in physical mixing, is surrounded by electrocatalysts particles. Thereby, the unique method established to synthetize the graphene using thermal expansion, aiming for a high purity material without contaminations of elements or chemical species common in synthesis using chemical reactants, was successfully achieved. Therefore, this different composition and morphology than mostly graphene materials could provide physical-chemical properties with high influences in electrochemical reactions.

Fig. 4 presents the cyclic voltammetry curves registered after 45 cycles of the comparing the electrocatalyst and physical mixing electrochemical activity. Fig. 4a shows the cyclic voltammetry in 0.5 M H_2SO_4; there is three main regions: the hydrogen from - 0.2 V to 0.1 V, double layer region between 0.1 V and 0.35 V and above 0.35 V the oxide species region. The $Pt_2Sn/C_{100\,\%}$ and $Pt_2Sn/C_{90\,\%} + G_{10\,\%}$ exhibit a higher desorption peak compared to others in the hydrogen region, furthermore hydrogen adsorption peak of $Pt_2Sn/C_{90\,\%} + G_{10\,\%}$ highlighting around - 0.1 V. Above 0.35 V, in the oxide species region the $Pt_2Sn/C_{100\,\%}$ and $Pt_2Sn/C_{90\,\%} + G_{10\,\%}$ show higher adsorption/desorption areas than other physical mixing, moreover $Pt_2Sn/C_{90\,\%} + G_{10\,\%}$ exhibits a desorption peak shift to a higher potential region (~ 0.52 V), the initial indication of graphene influences in the electrochemical activity. The cyclic voltammetry in 1.0 M NaOH is presented in Fig. 4b. The hydrogen region, - 0.9 V to - 0.65 V, exhibits a well-marked adsorption/desorption peaks to $Pt_2Sn/C_{100\,\%}$; forward to a narrowing in the double layer region, - 0.65 V to around - 0.45 V; above - 0.45 V there is oxide species region, $Pt_2Sn/C_{100\,\%}$ shows the higher area and well-marked peaks.

The capacitance calculated from geometrical area of voltammograms (Fig. 4a), decreases along with the increases of ethanol concentration (Table 3). The presence of ethanol can create diffusional barriers, increasing the interfacial resistance by the change in the viscosity and the conductive environment. Nevertheless, this effect should affect the capacitance similarly in both electrolytes, the changes in the acid were more acute, while alkaline electrolyte present a capacitance variation. The higher mobility and the protonation of oxygen-containing groups, e.g.–OH and –COOH, in acid tends to a thinner double layer enhancing the electrostatic interaction leading to a higher capacitance, while in the alkaline electrolyte OH^- ions along with oxygen-containing groups deprotonated increases the negative surface charge, expanding the double layer and decreasing the capacitance. Hence, the decrease of capacitance in acid with increase of ethanol concentration is due to the surface charge changes modifying the double layer; whilst in the alkaline exhibited a lower capacitance compared with acid, although its surface charges and double layer were more stable.

Beyond that, we need to pay attention to the composition of physical mixing, due total mass been set up as 5 mg, the increase in the graphene amount means a decrease in the amount of electrocatalyst ($Pt_2Sn/C_{100\,\%}$). That means $Pt_2Sn/C_{20\,\%} + G_{80\,\%}$ has 20 % of electrocatalyst in comparison to $Pt_2Sn/C_{100\,\%}$, and therefore 20 % of metal alloy amount of $Pt_2Sn/C_{100\,\%}$. This fact must be considered in our analysis. Thereby, Table 1 presents the mass weight of electrocatalyst and graphene in each physical mixing and the graphene ratio in relation to the electrocatalyst mass in the mixing. To obtain a more accurate analysis of the electrochemical activity, henceforward all data was normalized by platinum amount, allowing a comparison between the different physical mixing, and investigating the real influence of graphene powder as a booster to ethanol oxidation.

Table 3 exhibits the electrochemical active surface area (ECSA) calculated from the integrated area of the hydrogen adsorption peaks in the acid electrolyte cycle voltammogram form Fig. 4a, assuming 210 μC cm^{-2} value for hydrogen monolayer adsorption [37]. The graphene addition in physical mixing ($Pt_2Sn/C_{90\,\%} + G_{10\,\%}$) increases the ECSA in 47.4 % compared to $Pt_2Sn/C_{100\,\%}$. Forward the increasing of graphene amount, the ECSA decreases until the 40 % concentration ($Pt_2Sn/C_{60\,\%} + G_{40\,\%}$) when it starts to increase again with graphene increase. Despite the $Pt_2Sn/C_{10\,\%} + G_{80\,\%}$ exhibits the highest ECSA, this high value could be attributed to an anomaly caused by normalization, which high concentrations of graphene in physical mixing will require a data normalization by larger values, generating weird behaviors. Therefore, the most accurate results of normalization, which be attributed to the lowers concentrations of graphene, are less susceptible to the normalization error. Hence, $Pt_2Sn/C_{90\,\%} + G_{10\,\%}$ can be considered a valid result for obtain a 47.4 % increase while just have 11 % m/m ratio (Table 2), thus the normalization adjust does not have the majority influence in this case. Thence, $Pt_2Sn/C_{90\,\%} + G_{10\,\%}$ has the highest ECSA of all, and evidence of graphene affect in electrochemical activity.

Fig. 5 presents the cyclic voltammetry of the ethanol oxidation at four concentrations. Overall, we can notice the concentration effect, where current density increases together with ethanol concentration until 2.0 M, when it achieves a certain stability. We are aware that fuel rise as an approach to generate energy is limited by solution diffusional effects. The enhancement of current density by ethanol concentrations above 2.0 M is unreasonable. Therefore, we are going to establish the

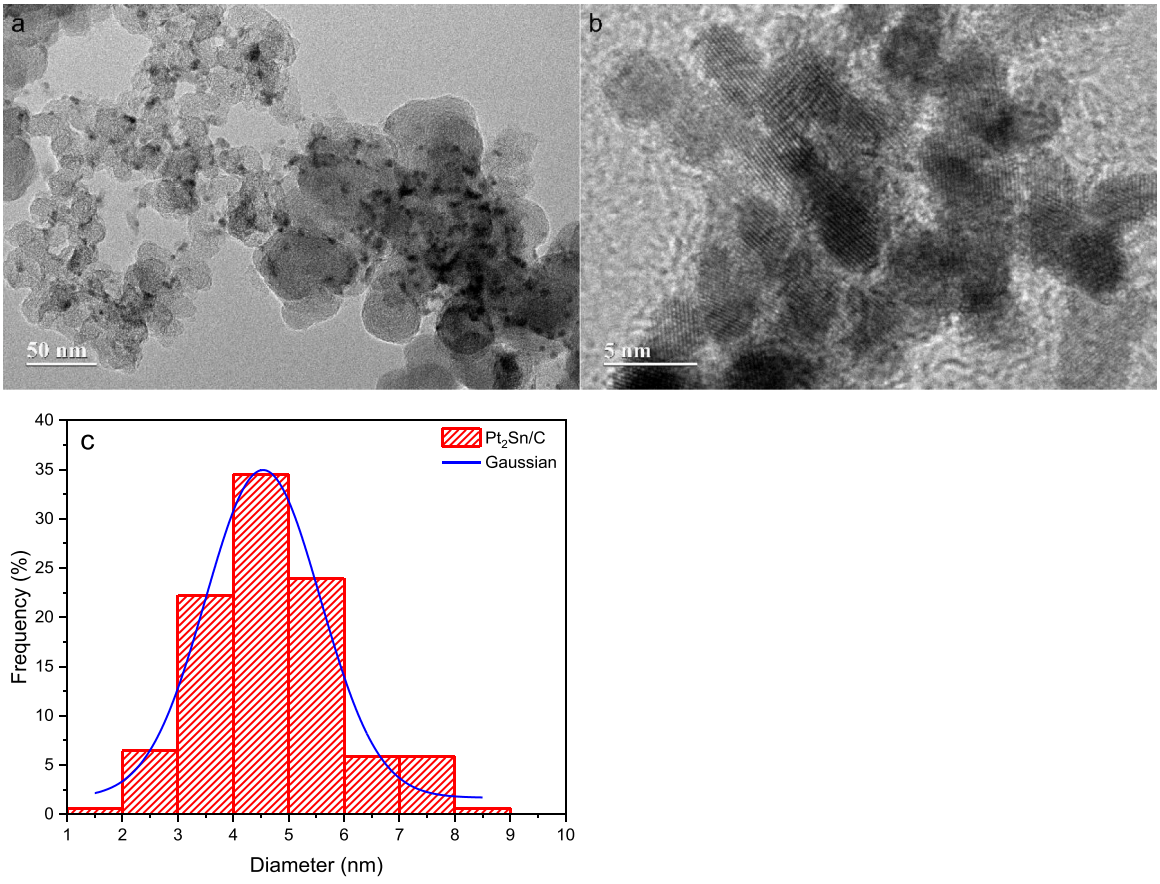

Fig. 2. (a) TEM (b) HRTEM and (c) histogram of the Pt_2Sn/C.

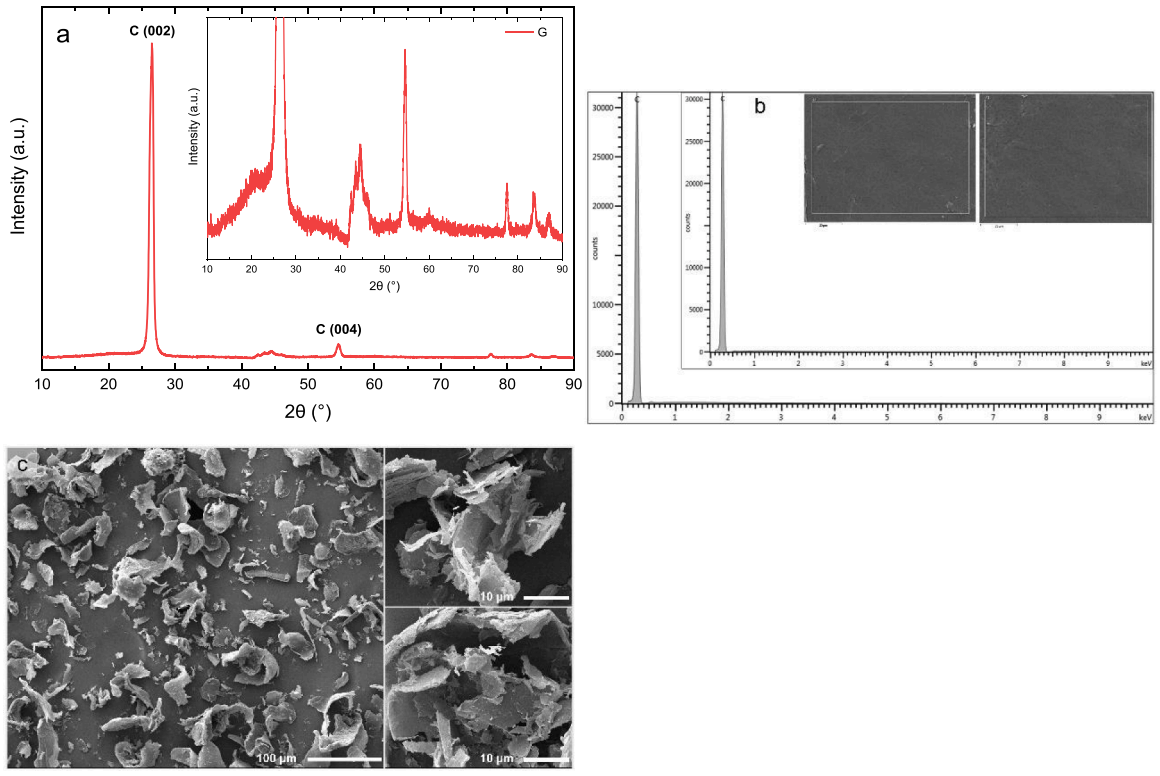

Fig. 3. (a) XRD, (b) EDS and (c) SEM of the graphene.

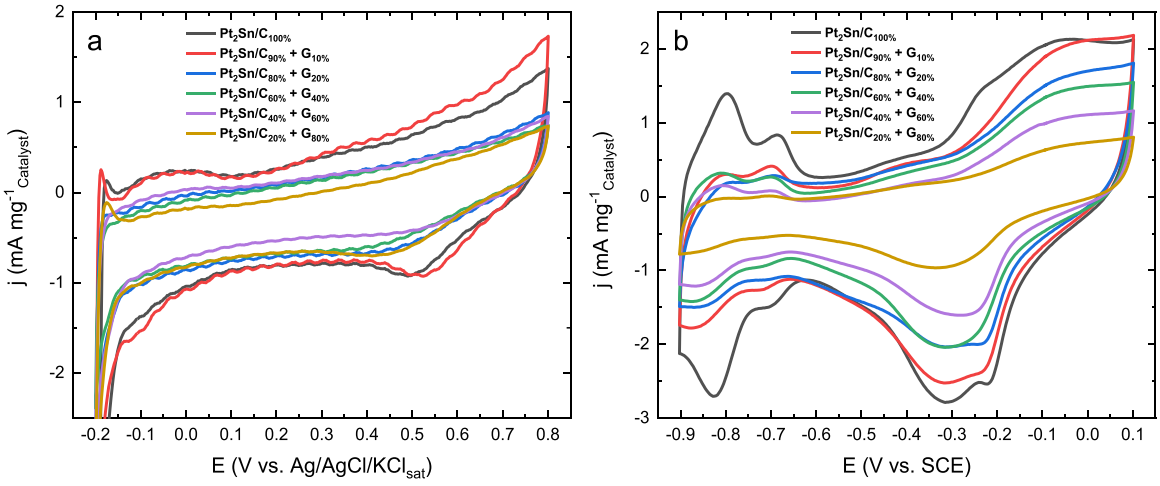

Fig. 4. Cyclic voltammetry Pt_2Sn/C in (a) H_2SO_4 0.5 M and (b) NaOH 1.0 M, scan rate 50 m V s^{-1}.

Table 3
ECSA of the hydrogen desorption and onset oxidation potential in 2.0 M ethanol.

Physical Mixing	ECSA / $cm^2\ mg^{-1}_{Pt}$	Onset oxidation		Capacitance	
		H_2SO_4 / V	NaOH / V	H_2SO_4 / $mF\ mg^{-1}_{Cat}$	NaOH / $mF\ mg^{-1}_{Cat}$
$Pt_2Sn/C_{100\,\%}$	37.07	0.286	−0.666	12.90	26.18
$Pt_2Sn/C_{90\,\%} + G_{10\,\%}$	54.63	0.292	−0.639	13.93	21.16
$Pt_2Sn/C_{80\,\%} + G_{20\,\%}$	11.83	0.317	−0.637	8.30	18.01
$Pt_2Sn/C_{60\,\%} + G_{40\,\%}$	8.70	0.324	−0.629	7.16	16.16
$Pt_2Sn/C_{40\,\%} + G_{60\,\%}$	23.97	0.312	−0.634	7.18	12.19
$Pt_2Sn/C_{20\,\%} + G_{80\,\%}$	94.65	0.295	−0.629	6.84	7.59

2.0 M as the best performance and use it to investigate the catalytic activity of physical mixing. The onset potential of the ethanol oxidation reaction (Table 3) was arbitrarily obtained where the current density was 1 % greater than the highest current from base cyclic voltammetry. In the acid electrolyte (Fig. 5), $Pt_2Sn/C_{100\,\%}$ presents the lower onset potential (Table 3) followed by $Pt_2Sn/C_{90\,\%} + G_{10\,\%}$ that obtained the lowest onset potential among the physical mixing, indicating a better performance than higher graphene concentrations. Table 4 shows the current density peak of the forward and backward scans of the 2.0 M ethanol oxidation (Fig. 5c). The addition of the graphene powder generates an increase in current density of 34.16 % and 57.18 % of the $Pt_2Sn/C_{90\,\%} + G_{10\,\%}$ and $Pt_2Sn/C_{20\,\%} + G_{80\,\%}$, respectively, in comparison with $Pt_2Sn/C_{100\,\%}$. We can notice that $Pt_2Sn/C_{80\,\%} + G_{20\,\%}$ and $Pt_2Sn/C_{60\,\%} + G_{40\,\%}$ exhibited the lowest current density. Likely, this poor performance is due to the decrease in the electrocatalyst amount, and consequently the metal alloy amount, which is fundamental to reasonable ethanol oxidation. Along with ECSA, these results showed that despite the graphene powder been only mixed, thus does not have metal particles in its surface. Its structure properties can provide an increase in the electrochemical activity of adsorption/desorption species, e.g. hydrogen desorption, which was used to calculate ECSA. Furthermore, the presence of graphene enhances the ethanol oxidation performance, suggesting that the graphene properties directly influence the chemical reactions. Analyzing the electrode preparation, the suspension deposition on the carbon glassy could create layers of the electrocatalyst and graphene stacked. This allowed graphene sheets closer to metal activity sites and assisting directly in the reactions. The graphene hexagonal structure with pi bonds enables high electron conductivity and adsorption/desorption properties. On the other hand, the increase in current density could be provided by adsorption of species releasing electrons to the electrical systema, although this behavior implies in current decrease in long operation tests, which is not seen in experimental data (Fig. 7). Thereby, the most accurate suggestion is the influence of graphene in the oxidation mechanism reaction of ethanol by their physical-chemical properties and needs to be deeply investigated.

Fig. 6 presents the cyclic voltammetry for ethanol oxidation in the alkaline electrolyte. Overall, the effect of current increase due to fuel concentration is seen as acid electrolyte. However, concentrations higher than 2.0 M are noticed a decrease of current, mainly in physical mixing with greater graphene amount, suggesting this effect is highly influenced by graphene. According to the Lewis definition, base chemical species act as electron donors. We can reckon that change in electrolyte provokes a different intermolecular interaction between the graphene sheets and the chemical species in the solution, e.g. stronger adsorptions or impediment of assistance in the reaction mechanism by graphene. Fig. 6c shows the oxidation of 2.0 M ethanol where $Pt_2Sn/C_{90\,\%} + G_{10\,\%}$ and $Pt_2Sn/C_{20\,\%} + G_{80\,\%}$ exhibit a current density of 10.48 % and 101.67 % higher than $Pt_2Sn/C_{100\,\%}$, respectively. On the other hand, $Pt_2Sn/C_{80\,\%} + G_{20\,\%}$ obtained a performance like $Pt_2Sn/C_{100\,\%}$, showing the influence of graphene powder in the catalytic activity reactions. Comparing the physical mixing, $Pt_2Sn/C_{90\,\%} + G_{10\,\%}$ has the lower onset oxidation (Table 3), this indicates that all reactions process has greater spontaneous to occur than using other physical mixing. Table 3 shows the onset potential increasing with the amount of graphene in the mixing. Using the current density peaks, we can calculate the ratio between the forward and backward scans, as shown in Table 4. This could be used as an indicative of the fuel oxidation rate. The ratios higher than one indicate that more reactions occurred in forward scan than in backward, suggesting an effective oxidation of ethanol. Unlike $Pt_2Sn/C_{100\,\%}$ all physical mixing presents a forward/backward scans ratio higher than 1, another stronger evidence of the graphene influence in the electrochemical reactions, even by only a physical interaction with the electrocatalyst, proving the method functionality to booster the ethanol oxidation.

Fig. 7 shows the chronoamperometry data from ethanol oxidation reaction at 0.3 V and - 0.2 V in acid and alkaline electrolytes, respectively. The current decreases asymptotically. In acid electrolyte (Fig. 7a), $Pt_2Sn/C_{90\,\%} + G_{10\,\%}$ present the highest final current density (8.42 $mA{\cdot}mg^{-1}_{Pt}$), showed in Table 5, an increase of 101.18 % in comparison to $Pt_2Sn/C_{100\,\%}$ (4.19 $mA{\cdot}mg^{-1}_{Pt}$). $Pt_2Sn/C_{80\,\%} + G_{20\,\%}$ (8.29 $mA{\cdot}mg^{-1}_{Pt}$) and $Pt_2Sn/C_{60\,\%} + G_{40\,\%}$ (6.51 $mA{\cdot}mg^{-1}_{Pt}$) also exhibited an increase of 98.00 % and 55.52 % in the final current compared to

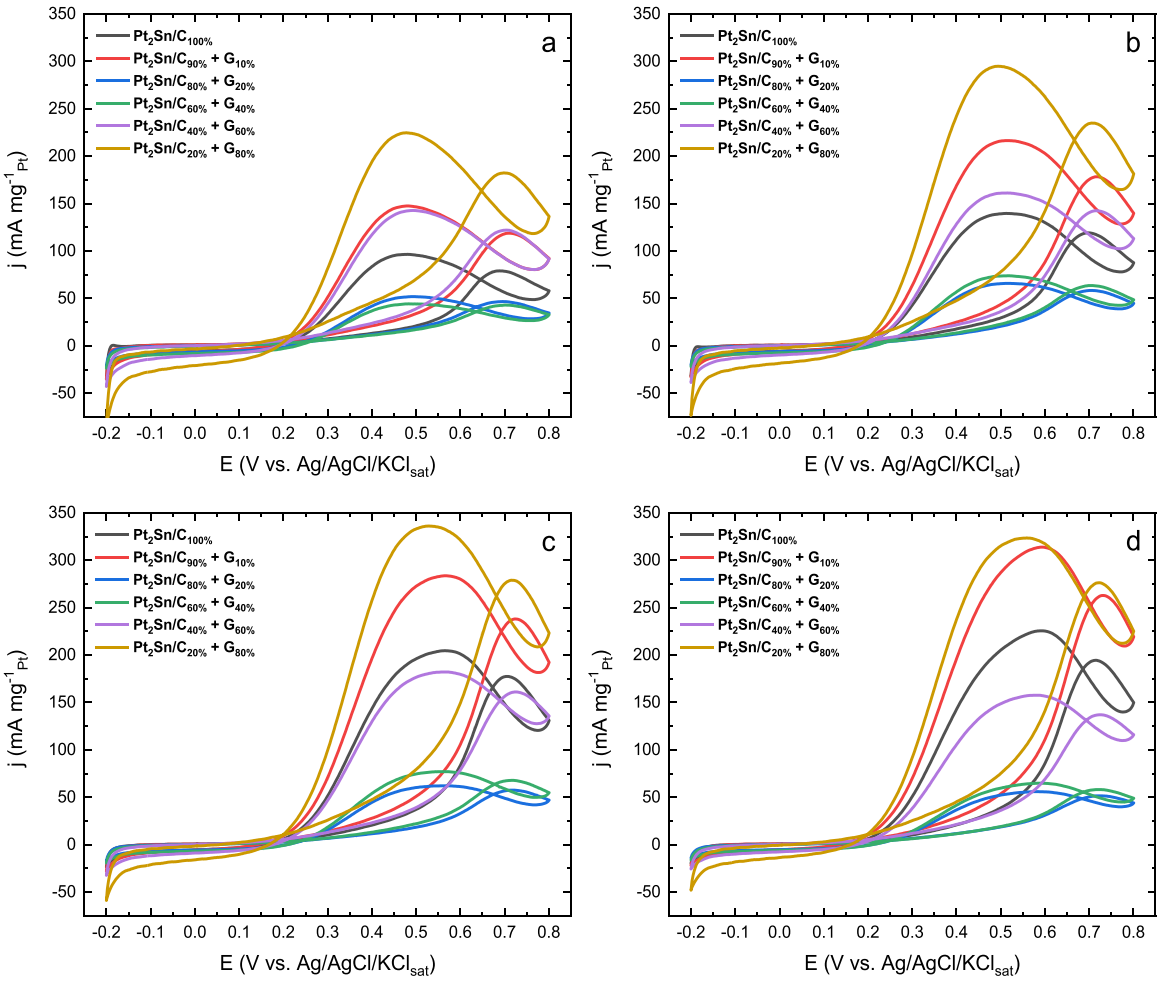

Fig. 5. Cyclic voltammetry of the Pt_2Sn/C and physical mixing in H_2SO_4 0.5 M with (a) 0.5 M, (b) 1.0 M, (c) 2.0 M and (d) 3.0 M ethanol concentration in the electrolyte, scan rate 50 m V s^{-1}.

Table 4
Current density peaks of ethanol oxidation reaction in forward scan, backward scan, and forward/backward scans ratio in 2.0 M ethanol.

	Physical Mixing	Forward peak mA mg_{Pt}^{-1}	Backward peak mA mg_{Pt}^{-1}	I_f/I_b
Acid electrolyte	$Pt_2Sn/C_{100\,\%}$	177.46	204.57	0.87
	$Pt_2Sn/C_{90\,\%} + G_{10\,\%}$	238.07	283.60	0.84
	$Pt_2Sn/C_{80\,\%} + G_{20\,\%}$	57.57	62.17	0.93
	$Pt_2Sn/C_{60\,\%} + G_{40\,\%}$	67.87	77.06	0.88
	$Pt_2Sn/C_{40\,\%} + G_{60\,\%}$	161.10	182.15	0.88
	$Pt_2Sn/C_{20\,\%} + G_{80\,\%}$	278.93	336.08	0.83
Alkaline electrolyte	$Pt_2Sn/C_{100\,\%}$	203.88	213.63	0.95
	$Pt_2Sn/C_{90\,\%} + G_{10\,\%}$	225.24	210.16	1.07
	$Pt_2Sn/C_{80\,\%} + G_{20\,\%}$	204.03	194.84	1.05
	$Pt_2Sn/C_{60\,\%} + G_{40\,\%}$	133.87	111.21	1.20
	$Pt_2Sn/C_{40\,\%} + G_{60\,\%}$	200.23	180.92	1.11
	$Pt_2Sn/C_{20\,\%} + G_{80\,\%}$	411.17	393.52	1.04

$Pt_2Sn/C_{100\,\%}$, respectively. Conversely, in alkaline electrolyte (Fig. 7b) only $Pt_2Sn/C_{90\,\%} + G_{10\,\%}$ (9.86 mA·mg_{Pt}^{-1}) and $Pt_2Sn/C_{20\,\%} + G_{80\,\%}$ (10.37 mA·mg_{Pt}^{-1}) have a final current density (Table 5) higher than $Pt_2Sn/C_{100\,\%}$ (9.17 mA·mg_{Pt}^{-1}), an increase of 7.53 % and 13.18 %, respectively. The inferior performance of physical mixing in alkaline chronoamperometry could be related directly to physical-chemical properties of graphene interaction with electrolyte.

The Cottrell curves shown in Figs. 7c and 7d reveals the direct effect of the graphene through the system. In both electrolytes there are deviations from ideal linear behavior characteristic of a pure diffusional process, affecting the alkaline system more intensively. Deviations (from linearity) in the region of short times (higher $t^{-1/2}$) can be related to adsorption and desorption of species, surface changes in the electrode, kinetic limitations, such as slow electron transfer, while in regions of long times (lower $t^{-1/2}$) deviations due to convective effect and diffusion layer dominate. Therefore, alkaline electrolyte led to a mass transfer slower than in acid. Considering that high levels of graphene amount in the mixing lead to extrapolation in normalized data, high levels of $G_{X\%}$ should be analyzed carefully. Thus, there is a clear limitation on mass transport of $Pt_2Sn/C_{90\,\%} + G_{10\,\%}$ and $Pt_2Sn/C_{80\,\%} + G_{20\,\%}$ in comparison to $Pt_2Sn/C_{100\,\%}$, consequently the enhance of the current of $Pt_2Sn/C_{X\%} + G_{X\%}$ mix in comparison to $Pt_2Sn/C_{100\,\%}$ can be related to adsorption and desorption of species and the charge transfer. The decrease in capacitance by the increase of graphene amount indicates a blocking surface and altering of interfacial dielectric, which can limit the charge transfer. The high amount levels of graphene are more susceptible to this phenomenon, mainly in alkaline electrolyte. The drop of current (Fig. 7a and b) from initial time achieving a steady state is led by the diffusion layer reaching a thickness where mass transport of reactant to the electrode equals its consumption rate. Through Cottrell equation, both systems (acid and alkaline electrolytes) under the same conditions, electrode area and bulk concentration, the current is proportional to diffusion, hence the changes in the current can be directly related to diffusion process. The region of short times in chronoamperometry (higher $t^{-1/2}$ in Cottrell curves) shown that current in alkaline electrolyte presents smaller variations than compared to acid while the $t^{-1/2}$

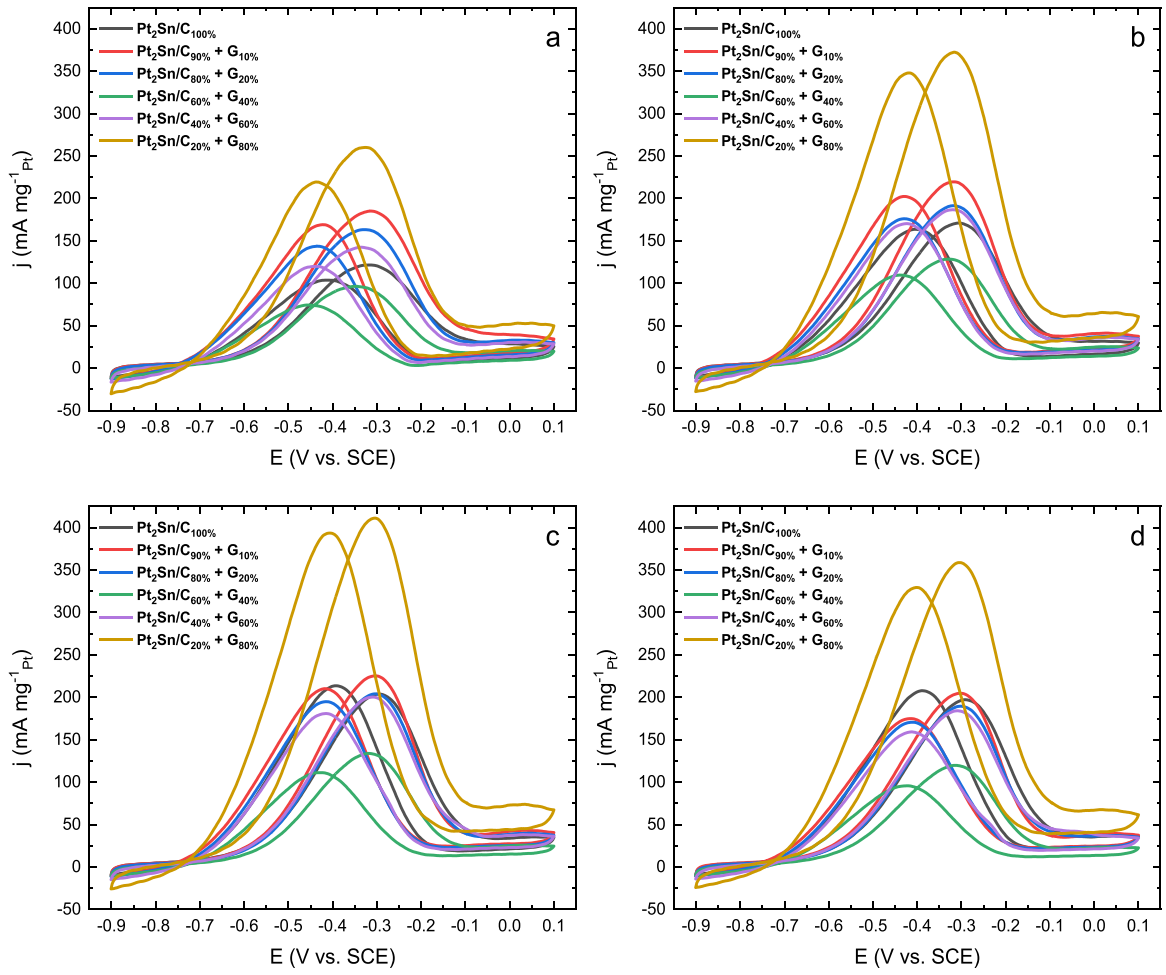

Fig. 6. Cyclic voltammetry of the Pt_2Sn/C and physical mixing in NaOH 1.0 M with (a) 0.5 M, (b) 1.0 M, (c) 2.0 M and (d) 3.0 M ethanol concentration in the electrolyte, scan rate 50 m V s^{-1}.

Table 5
Final current density and poisoning rate of the electrocatalysts from chronoamperometry.

Physical Mixing	j_{Final} (mA mg_{Pt}^{-1}) H_2SO_4	j_{Final} (mA mg_{Pt}^{-1}) NaOH	δ (% s^{-1}) Acid electrolyte	δ (% s^{-1}) Alkaline electrolyte
$Pt_2Sn/C_{100\,\%}$	4.19	9.17	0.02467	0.01870
$Pt_2Sn/C_{90\,\%}$ + $G_{10\,\%}$	8.42	9.86	0.01576	0.01830
$Pt_2Sn/C_{80\,\%}$ + $G_{20\,\%}$	8.29	5.16	0.01653	0.01839
$Pt_2Sn/C_{60\,\%}$ + $G_{40\,\%}$	6.51	7.92	0.02078	0.02173
$Pt_2Sn/C_{40\,\%}$ + $G_{60\,\%}$	4.64	7.49	0.01956	0.02295
$Pt_2Sn/C_{20\,\%}$ + $G_{80\,\%}$	0.68	10.37	0.03450	0.01598

decreases from 3.0 $s^{-1/2}$ till around 0.5 $s^{-1/2}$. As a result, in acid the current is strong domain by mass transport limitation. On the other hand, in alkaline electrode, the smooth variation in the current exhibited in Cottrell curve (Fig. 7d) whilst the sharp decrease in chronoamperometry (Fig. 7b) indicates a limitation effect by additional processes, e.g. double-layer charging and surface blockage by adsorption/desorption reaction intermediates during the initial time analysis.

Furthermore, aiming at the application of this method in fuel cells we should consider the higher relevance of durability and endurance of catalysts as for oxidation reactions in fuel cells. Table 5 shows the poisoning rate (δ) calculated from the chronoamperometry results by measuring the linear decay of the current for a period above t = 500 s using Eq. 2.

$$\delta = \frac{100}{i_0}\left(\frac{di}{dt}\right)_{t>500s} \quad (\%^{-1}) \tag{2}$$

Where $\left(\frac{di}{dt}\right)_{t>500s}$ is the slope of the linear portion of the current decay and i_0 is the current at the t = 0 obtained from polarization back extrapolated from linear current decay. The larger is the δ value larger is the poisoning effect of the catalysts[38]. Moreover, as mentioned before the proportion of graphene and electrocatalyst was used to normalize the data (Table 1). Thus, we also need to pay attention not only to the higher performance results, but also to the composition of physical mixing. What does its profit achieve a current density higher than other physical mixing if it is necessary use dozens or hundreds ratio more of graphene, as shown in Table 1. Hence, the highest performance, even in acid as in alkaline electrolyte, using the minimal necessary of graphene in the mixing was $Pt_2Sn/C_{90\,\%}$ + $G_{10\,\%}$, consequently the best composition to boost ethanol oxidations using platinum-tin electrocatalyst. The cycle voltammetry curves from pre and post chronoamperometry analyses (individual graphs in supporting information) also can provide additional information about catalyst degradation. In acid electrolyte $Pt_2Sn/C_{90\,\%}$ + $G_{10\,\%}$ presented a decrease of 28 % in the current density peak after chronoamperometry while $Pt_2Sn/C_{100\,\%}$ exhibited a 35 % decrease, similarity in alkaline, the reduction was 37 % and 41 %,

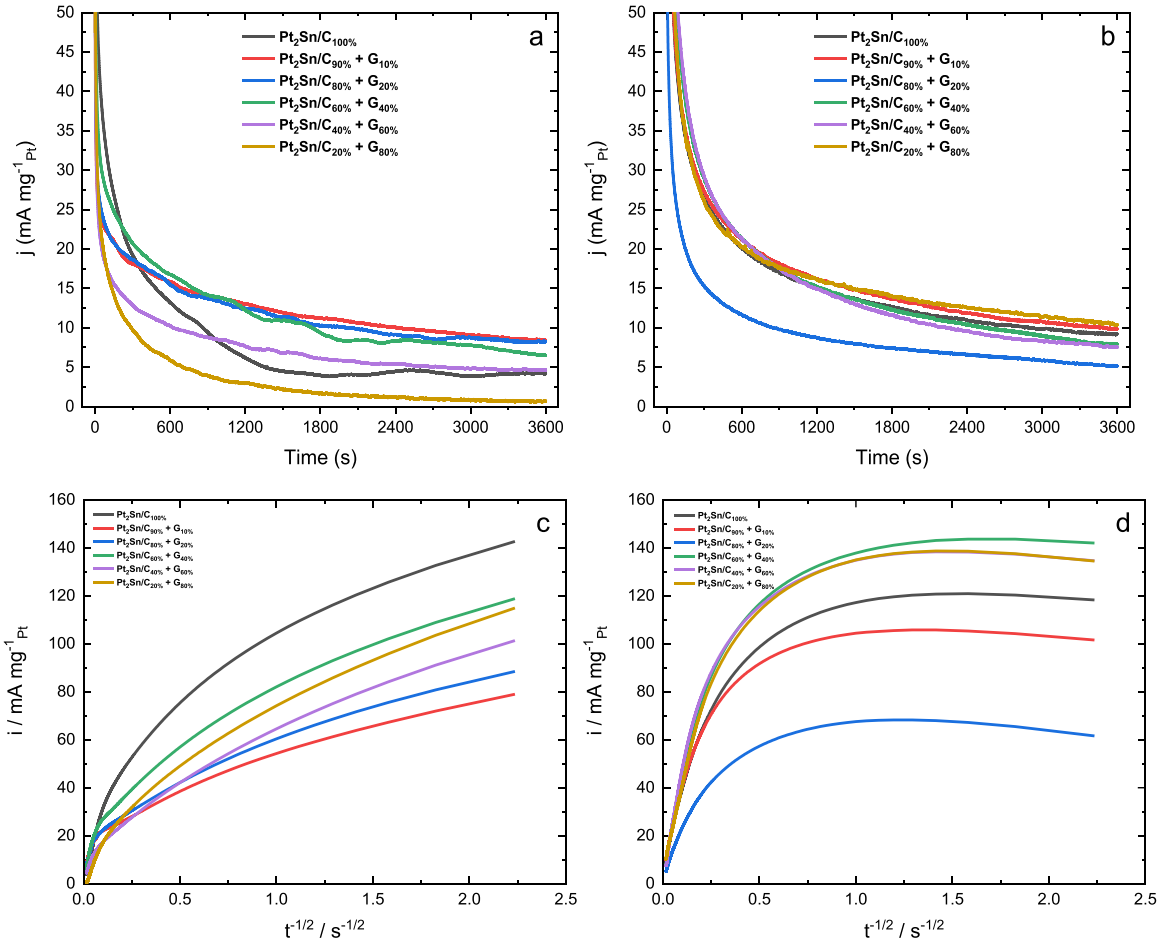

Fig. 7. Chronoamperometry of the Pt_2Sn/C and physical mixing in (a) H_2SO_4 0.5 M + 2.0 M ethanol, E = 0.3 V vs. $Ag/AgCl/KCl_{sat}$ and (b) NaOH 1.0 M + 2.0 M ethanol, E = -0.2 V vs. SCE, and Cottell curves obtained from the Chronoamperograms of (c) H_2SO_4 0.5 M + 2.0 M ethanol and (d) NaOH 1.0 M + 2.0 M ethanol.

respectively. This indicates that graphene presence by mix, in small amounts, i.e. 10 %, improves the endurance of the catalyst.

Overall, current density exhibited for alkaline electrolyte was higher than acid (Tables 4 and 5), indicating the influence of the OH– groups present in the solution and the characteristics of the graphene π bonds toward oxidation reactions. Furthermore, the tendency for current increases with increasing ethanol concentration achieves a limit of 2.0 M, which can be related to diffusional limitation or interfacial resistance by wettability change by ethanol presence, further affecting the conductive environment, double layer and dielectric properties. The wettability can be affected by ethanol molecules that have been absorbed on the surface; however, graphene remains largely hydrophobic in both acid and base, but in alkaline it can adsorb OH^- more strongly due to cation-π interactions, slightly improving wettability compared to acid [39,40]. Suggest that mass transport is affected by graphene layers, enhancing the electrochemical activity, using a limited graphene amount, i.e. 10 %, though high amounts lead to mass transport limitations and efficiency loss. Along with diffusion, the low electrical resistance of graphene and its influences in the charge transfer provoke the increase on the performance of mixing $Pt_2Sn/C_{90\,\%} + G_{10\,\%}$ in comparison with $Pt_2Sn/C_{100\,\%}$.

In comparison with similar approaches, the use of carbon nanotubes promotes enhance in oxidation endurance and improve conductivity and corrosion resistance playing against carbon Vulcan [41,42]. In a direct comparison with graphene, its 1D channels could provide superior mass transport in gas-phase catalyst compared to the diffusion of 2D graphene sheets [43,44]. However, its synthesis yields still pay a fetter to wide scale use, nevertheless, there is a lack of high-quality purification and common structural defects, which was overtaken by the thermal expansion method used to synthesize our graphene[45,46]. Another two-dimensional material which can be physically mixed with metal nanoparticles or catalysts is the MXenes. The use of it reports high yields toward oxidation ethanol reactions due to its synergistic conductivity and wide redox activity sites [47,48]. Although the enhances in stability, boosting long-term catalytic, and lowering the overpotentials for hydrogen and oxygen reactions, MXenes facilely restack reducing the layers' space obstructing the ions diffusion to the active sites [49,50]. Other disadvantages include the oxidation in aqueous or aerobic environments driving to formation of non-conductive and damaging catalyst-support interaction which weakens the electron transport[51,52]. At the same time, the production still faces challenges with standardization of the flaks, thickness and defects, lacking to scale production [53].

4. Conclusion

The electrocatalyst was successfully synthesized using a simple and straightforward method. The physical characterization analysis confirmed the presence of platinum and tin in the electrocatalyst metal alloy. The multilayers graphene obtained by an easy thermal expansion method, is pristine without any doping or elements addition, with high prospect of scalability, demonstrated its qualities and versatility in electrochemical application. Additionally, for the first time an increased performance method was reported using a physical mixing between electrocatalyst and graphene powder, without using metal addition nor chemical elements doping in graphene structure. The efficiency of

physical mixing was tested by cyclic voltammetry and chronoamperometry proving itself as superior to pure electrocatalyst, and $Pt_2Sn/C_{90\,\%} + G_{10\,\%}$ was the best proportion achieved, with superior performance in acid electrolyte. Thereby, physical mixing was proved as an alternative approach to enhance the catalytic activity of electrocatalyst in oxidation reactions, and further in fuel cell applications.

Declaration of Competing Interest

The authors declare that they have no known competing financial interests or personal relationships that could have appeared to influence the work reported in this paper

Acknowledgements

The authors gratefully acknowledge the financial support. FC thanks CNPq, grants 554569/2010–8, 475609/2008–5, 405793/2022-7 and FAPEG, grants 202110267000537, TLB thanks Capes from scholarship, 88887.701552/2022–00. RVG thank CNPq, grants 4, 302582/2021–5 and Fapemig, grant APQ-05247-23. Thanks also the Brazilian Institute of Science and Technology (INCT) in Carbon Nanomaterials and Nacional de Grafite Ltda.

Appendix A. Supporting information

Supplementary data associated with this article can be found in the online version at doi:10.1016/j.nxmate.2025.100807.

References

[1] R.M. Altarawneh, Overview on the vital step toward addressing platinum catalyst poisoning mechanisms in acid media of direct ethanol fuel cells (DEFCs), Energy Fuels 35 (2021) 11594–11612, https://doi.org/10.1021/acs.energyfuels.1c00453.
[2] M.S. Alias, S.K. Kamarudin, A.M. Zainoodin, M.S. Masdar, Active direct methanol fuel cell: an overview, Int J. Hydrog. Energy 45 (2020) 19620–19641, https://doi.org/10.1016/j.ijhydene.2020.04.202.
[3] Y. Yun, Alcohol fuels: current status and future direction. Alcohol Fuels - Current Technologies and Future Prospect, IntechOpen, 2020, https://doi.org/10.5772/intechopen.89788.
[4] E. Berretti, L. Osmieri, V. Baglio, H.A. Miller, J. Filippi, F. Vizza, M. Santamaria, S. Specchia, C. Santoro, A. Lavacchi, Direct alcohol fuel cells: a comparative review of acidic and alkaline systems, Electrochem. Energy Rev. 6 (2023) 30, https://doi.org/10.1007/s41918-023-00189-3.
[5] D. Wang, P. Wang, S. Wang, Y.-H. Chen, H. Zhang, A. Lei, Direct electrochemical oxidation of alcohols with hydrogen evolution in continuous-flow reactor, Nat. Commun. 10 (2019) 2796, https://doi.org/10.1038/s41467-019-10928-0.
[6] C. Coutanceau, S. Baranton, Electrochemical conversion of alcohols for hydrogen production: a short overview, WIREs Energy Environ. 5 (2016) 388–400, https://doi.org/10.1002/wene.193.
[7] J. Wang, S. Wasmus, R.F. Savinell, Evaluation of ethanol, 1-Propanol, and 2-Propanol in a direct oxidation Polymer-Electrolyte fuel cell: a Real-Time mass spectrometry study, J. Electrochem. Soc. 142 (1995) 4218–4224, https://doi.org/10.1149/1.2048487.
[8] C. Lamy, A. Lima, V. LeRhun, F. Delime, C. Coutanceau, J.-M. Léger, Recent advances in the development of direct alcohol fuel cells (DAFC), J. Power Sources 105 (2002) 283–296, https://doi.org/10.1016/S0378-7753(01)00954-5.
[9] M. Etesami, S. Mehdipour-Ataei, A. Somwangthanaroj, S. Kheawhom, Recent progress of electrocatalysts for hydrogen proton exchange membrane fuel cells, Int J. Hydrog. Energy 47 (2022) 41956–41973, https://doi.org/10.1016/j.ijhydene.2021.09.133.
[10] X. Shang, J.-H. Tang, B. Dong, Y. Sun, Recent advances of nonprecious and bifunctional electrocatalysts for overall water splitting, Sustain Energy Fuels 4 (2020) 3211–3228, https://doi.org/10.1039/D0SE00466A.
[11] L. Gong, Z. Yang, K. Li, W. Xing, C. Liu, J. Ge, Recent development of methanol electrooxidation catalysts for direct methanol fuel cell, J. Energy Chem. 27 (2018) 1618–1628, https://doi.org/10.1016/j.jechem.2018.01.029.
[12] Z. Xia, X. Zhang, H. Sun, S. Wang, G. Sun, Recent advances in multi-scale design and construction of materials for direct methanol fuel cells, Nano Energy 65 (2019) 104048, https://doi.org/10.1016/j.nanoen.2019.104048.
[13] E. Antolini, J. Perez, The renaissance of unsupported nanostructured catalysts for low-temperature fuel cells: from the size to the shape of metal nanostructures, J. Mater. Sci. 46 (2011) 4435–4457, https://doi.org/10.1007/s10853-011-5499-3.
[14] V. Mazumder, Y. Lee, S. Sun, Recent development of active nanoparticle catalysts for fuel cell reactions, Adv. Funct. Mater. 20 (2010) 1224–1231, https://doi.org/10.1002/adfm.200902293.
[15] L. Eswaraditya Reddy, D. Gollapudi, G. Mahnot Jain, S. Kolluru, G.V. Ramesh, Recent progress in the development of Platinum-based electrocatalysts for the oxidation of ethanol in fuel cells, Mater. Today Proc. 92 (2023) 636–641, https://doi.org/10.1016/j.matpr.2023.04.135.
[16] S. Jadali, M.A. Kamyabi, T. Alizadeh, The supported forest-like structure of PtSn as an effective deterrent for acetaldehyde formation during the electrocatalytic oxidation of ethanol, Fuel 325 (2022) 124780, https://doi.org/10.1016/j.fuel.2022.124780.
[17] Y. Yang, T. Yue, Y. Wang, Z. Yang, X. Jin, Effects of morphology on electrocatalytic activity of CeO2 nanomaterials, Microchem. J. 148 (2019) 42–50, https://doi.org/10.1016/j.microc.2019.04.051.
[18] Z. Chen, D. Higgins, Z. Chen, Electrocatalytic activity of nitrogen doped carbon nanotubes with different morphologies for oxygen reduction reaction, Electrochim. Acta 55 (2010) 4799–4804, https://doi.org/10.1016/j.electacta.2010.03.057.
[19] M.A. Alvi, M.S. Akhtar, An effective and low cost pd ce bimetallic decorated carbon nanofibers as electro-catalyst for direct methanol fuel cells applications, J. Alloy. Compd. 684 (2016) 524–529, https://doi.org/10.1016/j.jallcom.2016.05.101.
[20] C. Galeano, C. Baldizzone, H. Bongard, B. Spliethoff, C. Weidenthaler, J.C. Meier, K.J.J. Mayrhofer, F. Schüth, Carbon-Based Yolk–Shell materials for fuel cell applications, Adv. Funct. Mater. 24 (2014) 220–232, https://doi.org/10.1002/adfm.201302239.
[21] X. Peng, D. Lu, Y. Qin, M. Li, Y. Guo, S. Guo, Pt-on-Pd dendritic nanosheets with enhanced bifunctional fuel cell catalytic performance, ACS Appl. Mater. Interfaces 12 (2020) 30336–30342, https://doi.org/10.1021/acsami.0c05868.
[22] S. Hong, M. Hou, H. Zhang, Y. Jiang, Z. Shao, B. Yi, A high-performance PEM fuel cell with ultralow platinum electrode via electrospinning and underpotential deposition, Electrochim. Acta 245 (2017) 403–409, https://doi.org/10.1016/j.electacta.2017.05.066.
[23] J. Hou, M. Yang, C. Ke, G. Wei, C. Priest, Z. Qiao, G. Wu, J. Zhang, Platinum-group-metal catalysts for proton exchange membrane fuel cells: from catalyst design to electrode structure optimization, EnergyChem 2 (2020) 100023, https://doi.org/10.1016/j.enchem.2019.100023.
[24] Z. Qiao, S. Hwang, X. Li, C. Wang, W. Samarakoon, S. Karakalos, D. Li, M. Chen, Y. He, M. Wang, Z. Liu, G. Wang, H. Zhou, Z. Feng, D. Su, J.S. Spendelow, G. Wu, 3D porous graphitic nanocarbon for enhancing the performance and durability of pt catalysts: a balance between graphitization and hierarchical porosity, Energy Environ. Sci. 12 (2019) 2830–2841, https://doi.org/10.1039/C9EE01899A.
[25] O.O. Fashedemi, A. Bello, T. Adebusuyi, S. Bindir, Recent trends in carbon support for improved performance of alkaline fuel cells, Curr. Opin. Electrochem. 36 (2022) 101132, https://doi.org/10.1016/j.coelec.2022.101132.
[26] E. Antolini, Graphene as a new carbon support for low-temperature fuel cell catalysts, Appl. Catal. B 123–124 (2012) 52–68, https://doi.org/10.1016/j.apcatb.2012.04.022.
[27] N.T. Alvarez, P. Miller, M. Haase, N. Kienzle, L. Zhang, M.J. Schulz, V. Shanov, Carbon nanotube assembly at near-industrial natural-fiber spinning rates, Carbon N. Y 86 (2015) 350–357, https://doi.org/10.1016/j.carbon.2015.01.058.
[28] P.K. Adusei, S.N. Kanakaraj, S. Gbordzoe, K. Johnson, D. DeArmond, Y.-Y. Hsieh, Y. Fang, S. Mishra, N. Phan, N.T. Alvarez, V. Shanov, A scalable nano-engineering method to synthesize 3D-graphene-carbon nanotube hybrid fibers for supercapacitor applications, Electrochim. Acta 312 (2019) 411–423, https://doi.org/10.1016/j.electacta.2019.04.179.
[29] Z. Yang, J. Tian, Z. Yin, C. Cui, W. Qian, F. Wei, Carbon nanotube- and graphene-based nanomaterials and applications in high-voltage supercapacitor: a review, Carbon N. Y 141 (2019) 467–480, https://doi.org/10.1016/j.carbon.2018.10.010.
[30] H.-H. Huang, R.K. Joshi, K.K.H. De Silva, R. Badam, M. Yoshimura, Fabrication of reduced graphene oxide membranes for water desalination, J. Membr. Sci. 572 (2019) 12–19, https://doi.org/10.1016/j.memsci.2018.10.085.
[31] T.L. Bastos, R.V. Gelamo, F. Colmati, Carbon-graphene hybrid supporting platinum–tin electrocatalyst to enhance ethanol oxidation reaction, J. Appl. Electrochem. (2023), https://doi.org/10.1007/s10800-023-02027-2.
[32] T.L. Bastos, R.V. Gelamo, F. Colmati, The influence of carbon spheres and graphene synthesized by thermal method as platinum-tin electrocatalyst supports to enhance the ethanol oxidation, J. Solid State Electrochem. (2024), https://doi.org/10.1007/s10008-024-05980-w.
[33] L.G.B. Machuno, A.R. Oliveira, R.H. Furlan, A.B. Lima, L.C. Morais, R.V. Gelamo, Multilayer graphene films obtained by dip coating technique, Mater. Res. 18 (2015) 775–780, https://doi.org/10.1590/1516-1439.005415.
[34] U.V. Patil, A.S. Pawbake, L.G.B. Machuno, R.V. Gelamo, S.R. Jadkar, C.S. Rout, D. J. Late, Effect of plasma treatment on multilayer graphene: X-ray photoelectron spectroscopy, surface morphology investigations and work function measurements, RSC Adv. 6 (2016) 48843–48850, https://doi.org/10.1039/C6RA03046G.
[35] K. Hermann. Crystallography and Surface Structure, Wiley, 2011, 10.1002/9783527633296.
[36] H. Borchert, E.V. Shevchenko, A. Robert, I. Mekis, A. Kornowski, G. Grübel, H. Weller, Determination of nanocrystal sizes: a comparison of TEM, SAXS, and XRD studies of highly monodisperse CoPt 3 particles, Langmuir 21 (2005) 1931–1936, https://doi.org/10.1021/la0477183.
[37] T.J. Schmidt, H.A. Gasteiger, G.D. Stäb, P.M. Urban, D.M. Kolb, R.J. Behm, Characterization of High-Surface-Area electrocatalysts using a rotating disk electrode configuration, J. Electrochem. Soc. 145 (1998) 2354–2358, https://doi.org/10.1149/1.1838642.
[38] J.W. Guo, T.S. Zhao, J. Prabhuram, R. Chen, C.W. Wong, Preparation and characterization of a PtRu/C nanocatalyst for direct methanol fuel cells, Electro Acta 51 (2005) 754–763, https://doi.org/10.1016/j.electacta.2005.05.056.
[39] S. Wan, J. Pu, X. Zhang, L. Wang, Q. Xue, The tunable wettability in multistimuli-responsive smart graphene surfaces, Appl. Phys. Lett. 102 (2013) 011603, https://doi.org/10.1063/1.4775360.

[40] S. Yang, X. Zhao, Y.-H. Lu, E.S. Barnard, P. Yang, A. Baskin, J.W. Lawson, D. Prendergast, M. Salmeron, Nature of the electrical double layer on suspended graphene electrodes, J. Am. Chem. Soc. 144 (2022) 13327–13333, https://doi.org/10.1021/jacs.2c03344.
[41] J.C. Ortiz-Herrera, H. Cruz-Martínez, O. Solorza-Feria, D.I. Medina, Recent progress in carbon nanotubes support materials for Pt-based cathode catalysts in PEM fuel cells, Int J. Hydrog. Energy 47 (2022) 30213–30224, https://doi.org/10.1016/j.ijhydene.2022.03.218.
[42] K.J. Hughes, K.A. Iyer, R.E. Bird, J. Ivanov, S. Banerjee, G. Georges, Q.A. Zhou, Review of carbon nanotube research and development: materials and emerging applications, ACS Appl. Nano Mater. 7 (2024) 18695–18713, https://doi.org/10.1021/acsanm.4c02721.
[43] D.R. Kauffman, A. Star, Graphene versus carbon nanotubes for chemical sensor and fuel cell applications, Analyst 135 (2010) 2790, https://doi.org/10.1039/c0an00262c.
[44] S. Li, J. Shu, S. Ma, H. Yang, J. Jin, X. Zhang, R. Jin, Engineering three-dimensional nitrogen-doped carbon black embedding nitrogen-doped graphene anchoring ultrafine surface-clean pd nanoparticles as efficient ethanol oxidation electrocatalyst, Appl. Catal. B 280 (2021) 119464, https://doi.org/10.1016/j.apcatb.2020.119464.
[45] L.M. Esteves, H.A. Oliveira, F.B. Passos, Carbon nanotubes as catalyst support in chemical vapor deposition reaction: a review, J. Ind. Eng. Chem. 65 (2018) 1–12, https://doi.org/10.1016/j.jiec.2018.04.012.
[46] S. Li, L. Wu, J. Zhao, R. Li, H. Yang, L. Zhao, R. Jin, Nitrogen-doped carbon nanotubes embedded with nitrogen-doped carbon black anchoring pd nanocrystals to boost ethanol electrooxidation, Green Chem. 25 (2023) 10033–10042, https://doi.org/10.1039/D3GC02801A.
[47] L. He, H. Zhuang, Q. Fan, P. Yu, S. Wang, Y. Pang, K. Chen, K. Liang, Advances and challenges in MXene-based electrocatalysts: unlocking the potential for sustainable energy conversion, Mater. Horiz. 11 (2024) 4239–4255, https://doi.org/10.1039/D4MH00845F.
[48] I.H. Sajid, M.Z. Iqbal, S. Rizwan, Recent advances in the role of MXene based hybrid architectures as electrocatalysts for water splitting, RSC Adv. 14 (2024) 6823–6847, https://doi.org/10.1039/D3RA06725D.
[49] Q. Zhang, C. Zhao, H. Li, Synthesis and design strategies of MXene used as catalysts, ChemCatChem 16 (2024), https://doi.org/10.1002/cctc.202400917.
[50] L. He, H. Zhuang, Q. Fan, P. Yu, S. Wang, Y. Pang, K. Chen, K. Liang, Advances and challenges in MXene-based electrocatalysts: unlocking the potential for sustainable energy conversion, Mater. Horiz. 11 (2024) 4239–4255, https://doi.org/10.1039/D4MH00845F.
[51] L. He, H. Zhuang, Q. Fan, P. Yu, S. Wang, Y. Pang, K. Chen, K. Liang, Advances and challenges in MXene-based electrocatalysts: unlocking the potential for sustainable energy conversion, Mater. Horiz. 11 (2024) 4239–4255, https://doi.org/10.1039/D4MH00845F.
[52] A. Hamzehlouy, M. Soroush, MXene-based catalysts: a review, Mater. Today Catal. 5 (2024) 100054, https://doi.org/10.1016/j.mtcata.2024.100054.
[53] M. Kaleem Shabbir, F. Arif, H. Asghar, S. Irum Memon, U. Khanum, J. Akhtar, A. Ali, Z. Ramzan, A. Aziz, A.A. Memon, K. Hussain Thebo, Two-dimensional MXene-based electrocatalysts: challenges and opportunities, Chem. Rec. 24 (2024), https://doi.org/10.1002/tcr.202400047.